La Société Savante de l'Aéronautique et de l'Espace

50h 3AF International Conference on Applied Aerodynamics 29-30 March – 01 April 2015, Toulouse - France

FP36-2015-vanharen

TWO-DIMENSIONAL SPECTRAL ANALYSIS OF NONCONFORMING GRID INTERFACE. EMPHASIS ON UNSTEADY FLOWS.

Julien Vanharen [(1)], Guillaume Puigt [(2)], Marc Montagnac [(3)]

[(1)] Centre Européen de Recherche et de Formation Avancée en Calcul Scientifique, CFD team, 42 avenue Gaspard Coriolis, 31057 Toulouse Cedex 01, France, Email: julien.vanharen@cerfacs.fr
[(2)] Centre Européen de Recherche et de Formation Avancée en Calcul Scientifique, CFD team, 42 avenue Gaspard Coriolis, 31057 Toulouse Cedex 01, France, Email: guillaume.puigt@cerfacs.fr
[(3)] Centre Européen de Recherche et de Formation Avancée en Calcul Scientifique, CFD team, 42 avenue Gaspard Coriolis, 31057 Toulouse Cedex 01, France, Email: marc.montagnac@cerfacs.fr

ABSTRACT

A general framework is proposed to study the unsteady behaviour of nonconforming grid interface between two structured blocks. Using the Finite Volume Method, a two-dimensional spectral analysis is performed for a second order centred scheme to compare with solutions obtained by the ***elsA*** software. The nonconforming grid interface makes possible to coarse/refine each block, which is not without effect on both stability and accuracy of the unsteady solution. High coarsening is responsible for instabilities in the form of reflection of high-frequency waves at the nonconforming grid interface. This problem is solved using a high-order interpolation, which depends on metric, and a Riemann solver.

1. INTRODUCTION

During the last forty years, Computational Fluid Dynamics (CFD) has entered industry for the design of aircraft or turbomachinery. After solving Euler equations in 2D and in 3D with a Finite Volume approach, the increase in computational power has allowed to solve the Reynolds Averaged Navier-Stokes equations. With this approach, turbulence effects are averaged and only the mean effects are computed. Industrial flows are defined at large Reynolds number and turbulence must be accounted for. In order to capture accurately turbulence effects, the tendency was to consider structured meshes and to align mesh lines with the flow anisotropy, especially in the boundary layer. After thousands of computations, industry has been able to propose best practices in order to attain the best accuracy possible but at a moderate computational cost. In other words, the solvers were very accurate once the mesh followed some rules. As it has ever been suggested, the key point regarding computations was the definition of the mesh. Structured solvers are numerically very efficient since data are accessed easily but the mesh generation is the bottleneck. A structured mesh is built by dividing the domain of interest in several hexahedral blocks (this is called a topology) in which cells are referred by a triplet *(i, j, k)*, following the three directions defining the hexahedral block. One of the most famous mesh tools is called ICEM-CFD from Ansys. Initially, even if the mesh decomposition may need several days or weeks, the fact that the geometry was more or less the same (cruise version of an aircraft…) helped industries to define best practices for a topology and then to discretize the domain from this topology. For parametric studies, the global cost was acceptable regarding time spent for computations. The next tendency consisted in computing the flow around an object not at cruise conditions. For an aircraft, it means that the geometrical complexity is so large that industry is not able to afford the expense and several works have began in order to simplify the mesh generation process. Many approaches have been considered: the Chimera method [3], the hybrid approach [4], the DRAGON grid [5], the unstructured grid [2] and the nonconforming grid

interfaces [6]. The bottleneck of structured mesh generation process is the time-consuming topology and the fact that mesh lines go across any block interface. A solution is simply to authorize a parallel human being mesh generation process. The idea is simple: the computational domain is divided in certain large parts (wing, HTP, VTP, fuselage...) separated by predefined surfaces added to the CAD.

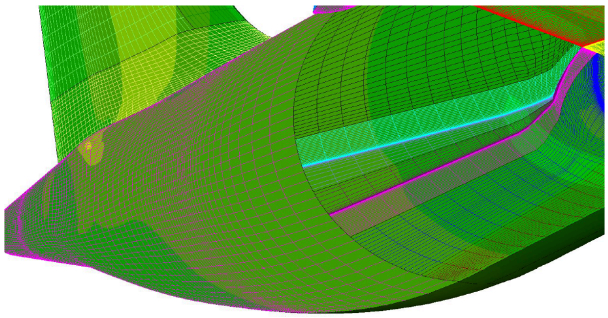

Figure 1. Nonconforming grid interface with a high coarsening to avoid propagating the mesh lines of the wing wake.

Using those surfaces, the initial domain is split into several subdomains and any subdomain is meshed independently. The principle of non-matching joins is to authorize two different discretizations on both sides of the surface. Hence, the zones limits are topologically identical but in practice, their discrete representations may differ. The final time for mesh generation is obviously decreased because several people can work in parallel on separated parts of the final mesh. The challenge concerns data exchange at the non-matching join. Our approach consists in defining intersection facets and to treat those facets as with a classical Finite Volume approach. The key point is therefore transferred to the facets definition. A geometric algorithm is considered for the definition of the facets and in our approach, the treatment is conservative once the intersection surfaces are planar. A lot of studies about theoretical foundations can be found in the literature. Rai [7, 8, 9] firstly introduced the nonconforming grid interface. They were used by Biedron [10] to compute the F-18 forebody with actuated control strake and by Epstein [19] to compute a generic wing. Rumsey [20] used the nonconforming grid interface to compute acoustic waves through sliding-zone interfaces. Lerat [17] studied their stability for the steady compressible Euler equations. Nonconforming approach has been introduced (historically) as a way to glue two domains that share a CAD surface. By essence, it was necessary to discretize both sides with comparable discretization parameters. But industry also found in non-matching interface a good way to decrease the computational time of Unsteady Reynolds Average Navier-Stokes simulations (URANS). In Fig. 1, the nonconforming grid interface after the C-grid around the wing allows to decrease the number of degrees of freedom. Nowadays, this kind of mesh is considered for steady polar computations and the industrial tendency is to also treat unsteady flows. As an example, this kind of mesh can be used to compute the gust response, which is clearly an unsteady phenomenon. For unsteady simulations, nonconforming grid interface are a good way to introduce larger cells in the mesh and therefore to allow larger time steps. Finally, computation robustness is increased while the computational cost is decreased. This is important for an industry when several hundreds of unsteady computations are performed each month. Large Eddy Simulation (LES) is the new kind of simulation to enter industry. RANS and URANS approaches are not able to capture accurately turbulence effects and as a consequence turbulence-driven phenomenon. LES consists in computing the largest turbulence scales and in modelling the lowest scales. The largest scales depend on the geometry, while the smallest ones are linked with dissipation by viscous effects. The largest scale effects are new interesting information to add to the industrial process. Among the phenomenon of potential interest, one can consider the flow at landing or take-off conditions, thermal protection system design... The main default of nonconforming grid interface is that they have been developed for steady simulations and simply extended to unsteady simulations without analysing their effect on unsteady phenomena. This is surprising: many efforts concern the measure of temporal and spatial accuracy of numerical schemes. But the scientific community generally forgets to analyse boundary conditions treatment. The aim of the present work is to study the nonconforming grid interface and its stability when used in unsteady simulations (Unsteady Reynolds Averaged Navier-Stokes, LES with low-order schemes) on multi-domain and multi-scale meshes. Given the success of this numerical method, it was already implemented inside the ***elsA*** software [23] without knowing the limits of the method in unsteady simulations (URANS or LES) on multi-domain and multi-scale meshes. This analysis must be performed theoretically and numerically on a simple configuration. In this paper, computations with the COnvection VOrtex (CO-VO) test case have been carried out. The CO-VO test case consists in transporting a vortex by advection and

it is easy to compare numerical and analytical reference solutions. The present work is divided into three parts. The first one presents the theoretical aspects of nonconforming grid interface. Analytical expressions are given to study stability in unsteady simulations (URANS). The second one studies the nonconforming grid interface on a non-uniform grid. In certain case, one can observe undesirable high-frequency waves reflection. Finally, the last one proposes solutions to improve significantly the unsteady treatment. A lot of solutions are considered in the literature to avoid the reflection. The first type of method consists in improving the spectral resolution. Berland [18] proposed explicit high-order numerical schemes for the accurate computation of multiple-scale problems and for the implementation of boundary conditions. Lele [15], Kim [16] and Fosso [22] compared compact schemes with well-known schemes based on Taylor series expansions. Bogey [25] and Tam [24] proposed explicit numerical methods by minimizing the dispersion and the dissipation errors in the wavenumber space (DRP schemes). The aim is to compute flow and noise with high accuracy and fidelity. The second type of method deals with improving the unsteady behaviour of boundary conditions. Based on the work of Thompson [21], Poinsot and Lele [14] developed the Navier-Stokes Characteristic Boundary Conditions, which is a Riemann solver. Kim and Lee [27, 28] used them to reduce spurious modes at block interfaces. In this paper, the unsteady behaviour is improved using a high-order interpolation, which depends on metric, and a Riemann solver. For further details, the reader will refer to [1].

2. 2D SPECTRAL ANALYSIS

The main aim of this paper is to illustrate a theoretical framework to analyse the nonconforming grid interface. Since stability analysis on the full Navier-Stokes equations is difficult, the advection equation with a constant velocity is only considered. The spatial derivative needs to be discretized. The spectral analysis of such interface must be carried out in two dimensions because the nonconforming grid interface only exists in two dimensions. For sake of clarity, the spatial discretization is described using the Cartesian toy mesh represented on Fig. 2. This latter is composed of two blocks, a right one and a left one, separated by a nonconforming grid interface. Using the classical Finite Volume Method to discretize the partial derivative with respect to the *x*-axis, one obtains Eq. 1.

$$\left.\frac{\partial f}{\partial x}\right|_{i,j} = \frac{f_{i+1/2,j} - f_{i-1/2,j}}{\Delta x_L}. \quad (1)$$

A numerical scheme is then necessary to evaluate the value at the interface. A second order scheme is used as in [29]. The left state interpolation $f_{i-1/2,j}$ is simply given by Eq. 2 since the stencil does not cross the interface.

$$f_{i-1/2,j} = \frac{f_{i,j} + f_{i-1,j}}{2}. \quad (2)$$

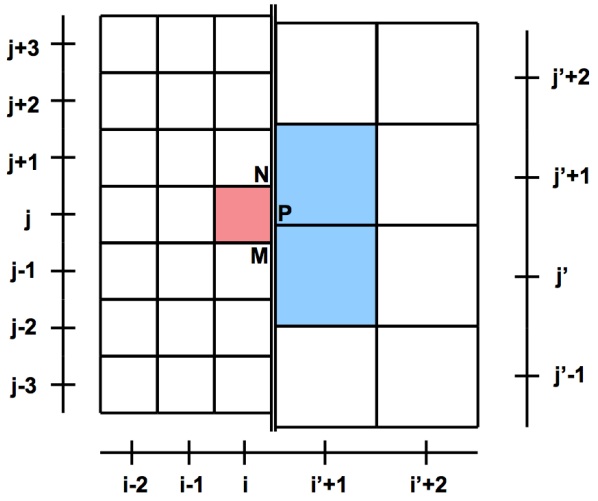

Figure 2. The toy mesh is composed of two blocks. The spatial discretization of the left (resp. right) block is ($\Delta x_L, \Delta y_L$) (resp. ($\Delta x_R, \Delta y_R$)). Both blocks are separated by the nonconforming block interface.

However, for the right state interpolation, the stencil does cross the interface and then, applying the numerical scheme is more complicated since the flux has to be weighted by the intersection surfaces in common between cells:

$$f_{i+1/2,j} = \frac{MP}{MN} f_{MP} + \frac{PN}{MN} f_{PN}. \quad (3)$$

Then, the second order scheme could be applied Eqs. 4-5.

$$f_{MP} = \frac{f_{i,j} + f_{i'+1,j'}}{2}. \quad (4)$$

$$f_{PN} = \frac{f_{i,j} + f_{i'+1,j'+1}}{2}. \quad (5)$$

By injecting Eqs. 2-3-4-5 into Eq. 1, one obtains Eq. 6.

$$\left.\frac{\partial f}{\partial x}\right|_{i,j} = \frac{f^{*}_{i+1,j} - f_{i-1,j}}{2\Delta x_L}. \tag{6}$$

where

$$f^{*}_{i+1,j} = \frac{MP}{MN} f_{i'+1,j'} + \frac{PN}{MN} f_{i'+1,j'+1}. \tag{7}$$

Let us assume that f is a normal mode to do a spectral analysis where I is the imaginary unit. k is the wavenumber. k_x (resp. k_y) is the projection of the wave vector on the x- (resp. y-) axis.

$$f_{i,j} = \exp\left[I\left(k_x i\Delta x_L + k_y j\Delta y_L\right)\right]. \tag{8}$$

Substituting Eq. (8) in (7), one obtains Eq. (9).

$$f^{*}_{i+1,j} = \left(1 - \frac{MP}{MN}\right)\exp\left[\begin{array}{l} Ik_x\left(\left(i+\frac{1}{2}\right)\Delta x_L \right. \\ \left. +\frac{\Delta x_R}{2}\right) \\ +Ik_y\left(j\Delta y_L + \frac{\Delta y_R}{2}\right. \\ \left. -\frac{\Delta y_L}{2} + MP\right) \end{array}\right] + \frac{MP}{MN}\exp\left[\begin{array}{l} Ik_x\left(\left(i+\frac{1}{2}\right)\Delta x_L \right. \\ \left. +\frac{\Delta x_R}{2}\right) \\ +Ik_y\left(j\Delta y_L - \frac{\Delta y_R}{2}\right. \\ \left. -\frac{\Delta y_L}{2} + MP\right) \end{array}\right]. \tag{9}$$

This concludes the discretization for the partial derivative with respect to the x-axis. The discretization along the y-axis is easier since the stencil never crosses the nonconforming grid interface. So, one classically obtains Eq. 10.

$$\left.\frac{\partial f}{\partial y}\right|_{i,j} = \frac{f_{i,j+1} - f_{i,j-1}}{\Delta y_L} = If_{i,j}\sin\left(k_y\Delta y_L\right)/\Delta y_L. \tag{10}$$

In the following, a von Neumann or a Fourier analysis is performed to highlight characteristics of the nonconforming grid interface in terms of amplification and dispersion. Naturally, the procedure is described for a cell, which belongs to the left block, but the same approach could be used to obtain relations for the right block. This is why, in the following, the superscript L (resp. R) refers to quantities evaluated for the left (resp. right) cell. The modified wavenumber along the x- (resp. y) axis is defined by Eqs. 11-12.

$$\kappa_x := \frac{1}{If_{i,j}}\left.\frac{\partial f}{\partial x}\right|_{i,j}. \tag{11}$$

$$\kappa_y := \frac{1}{If_{i,j}}\left.\frac{\partial f}{\partial y}\right|_{i,j}. \tag{12}$$

Eqs. 11-12 give two modified wavenumbers κ_x and κ_y, which is difficult to interpret in terms of amplification and dispersion. This is why A and φ are defined such that A represents dissipation and amplification and φ represents the dispersion error [1].

$$A\left(\Delta x\right) = \exp\left[\mathrm{Im}\left[\kappa_x + \kappa_z\right]\Delta x\right]. \tag{13}$$

$$\varphi\left(\Delta x\right) = \frac{k_x + k_y - \mathrm{Re}\left(\kappa_x + \kappa_y\right)}{\pi}\Delta x. \tag{14}$$

The functions A and φ are defined for all Δx in [0; π] to comply the Nyquist-Shannon theorem. The dispersion error is given by φ and the amplification by A. If $A > 1$, there is amplification and if $A < 1$, there is dissipation. Just remind that amplification means instability for the computation. The spectral analysis in two-dimension is then simply possible by plotting both functions. Since the discretization is different for each block, this means that it exists an amplification function and a dispersion function for the left block (A^L, φ^L) and the right block (A^R, φ^R). If the spatial discretization is different for each block, this means that A and φ are not defined on the same set to comply the Nyquist-Shannon theorem.

3. STABILITY AND ACCURACY

To confirm the results given by the analytical expressions, all computations have been carried out with the ***elsA*** software [23]. The test case deals with the convection of an isentropic and compressible vortex inspired by the High-Order Workshop [26], which is an analytical solution of unsteady compressible Euler equations. The flow is initialized with:

$$\begin{cases} u = U_0 - \beta U_0 \left(y - y_C\right) / R_C \exp\left(-r^2/2\right), \\ v = \beta U_0 \left(x - x_C\right) / R_C \exp\left(-r^2/2\right), \\ T = T_0 - 1/2 \left(\beta U_0\right)^2 \exp\left(-r^2\right) / C_p, \end{cases} \quad (15)$$

where p_0 = *101325.0 [Pa]*, T_0 = *300.0 [K]*, M_0 = *0.1 [-]*, R_C = *0.1 [m]* and the maximum velocity fluctuation u_{max} = *1.5 [m/s]*. The vortex reaches its maximum of fluctuation of pressure at x_C = *0.5 [m]* and y_C = *0.5 [m]*. As shown in Fig. 3, the vortex is perfectly convected. In this paper, the direction of propagation is always orthogonal to the grid interface but several tests have been done in [1] with a non-orthogonal direction of propagation.

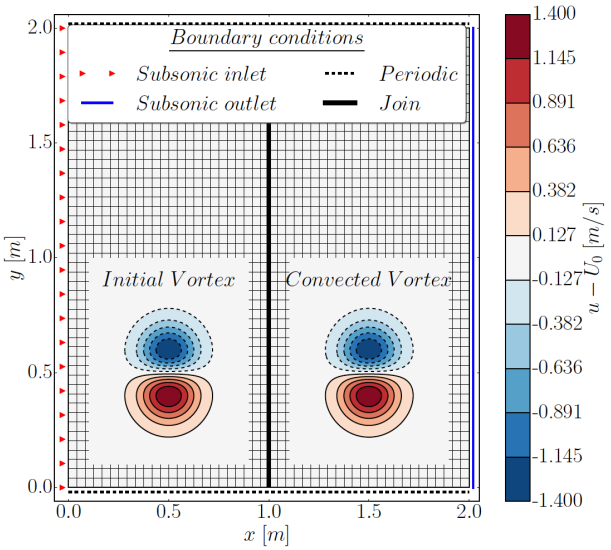

Figure 3. Coarse reference mesh and its boundary conditions (left block 25 x 5 x 50, right block 25 x 5 x 50). The vortex is convected from the left block to the right block.

In this paper, only the coarsening along the *x*-axis is examined. Please see [1] for further details and in particular the effect of the coarsening along the *y*-axis and the error analysis. Let us introduce $u = \Delta x_R / \Delta x_L$ which characterizes the coarsening. A spectral analysis have been performed for many test cases: *u = 1*, *2* or *4* and *h = 0.0* or *0.5*. If *h = 0.0*, the grid interface is conforming and the coarsening along the *x*-axis is responsible for dispersion and amplification. In general, *u > 1* implies instability.

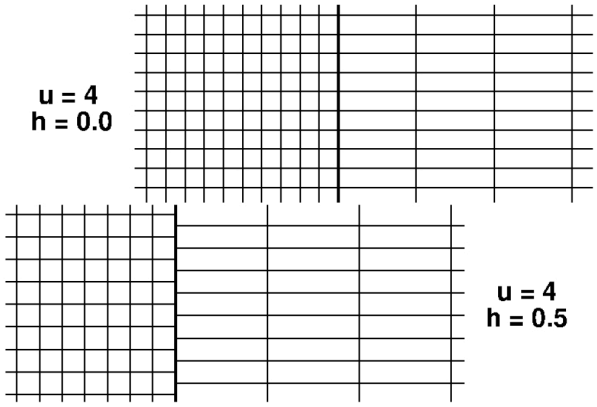

Figure 4. Examples of meshes with a nonconforming grid interface (h = 0 implies a conforming grid interface, h = 0.5 implies a nonconforming grid interface) and a coarsening (u = 4) along the x-axis.

Fig. 6 represents the *y*-component of the velocity fluctuation for different coarsening aspect ratio. Whether the grid interface is conforming or nonconforming, one obtains the same result. Instabilities are generated by the coarsening and not by the nonconforming interface. The coarsening generates a second kind of instabilities. It is responsible for high frequency waves reflection as shown in Fig. 7. Such a high coarsening ratio is often encountered in the industry as shown in Fig. 1. This reflection was *a priori* unexpected. Indeed, since the right block is coarse, one could expect that the vortex may be dissipated but without contamination of the upstream flow. This pollution is caused by the high coarsening ratio and not by the nonconforming grid interface. The only crime of the nonconforming grid interface is to allow such high coarsening ratio. This phenomenon has been widely studied by Vichnevetsky [11, 12, 13], in which wave analysis has been performed for one-dimensional problem (boundary conditions and mesh refinement). He has decomposed any solution as a sum of *p* and *q* waves, with *p* waves traveling in the hyperbolic direction (positive group velocity) and *q* waves in the opposite direction (negative group velocity). The *q* waves are not necessary present in the flow but they can appear in the case of mesh coarsening and boundary conditions not adapted.

The metric discontinuity modifies the dispersion relation as shown in Fig. 5.

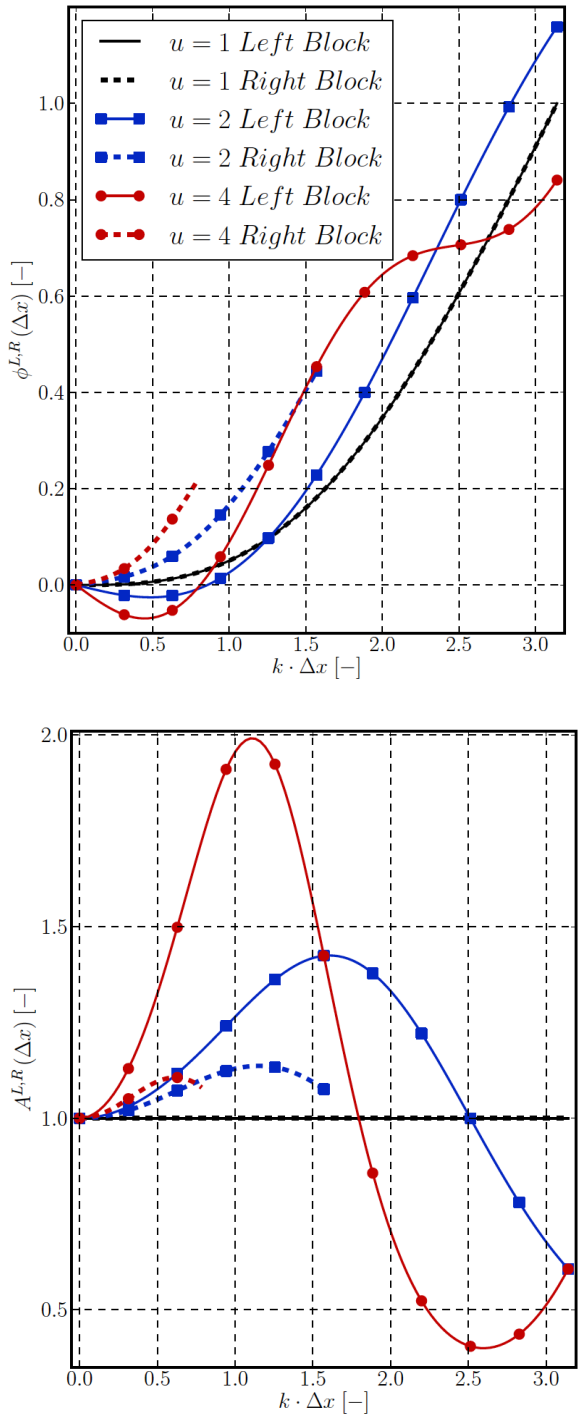

Figure 5. Dispersion and amplification for different coarsening ratio u. Solid lines represent the left block. Dash lines represent the right block. No matter what the value of h is, one obtains the same results.

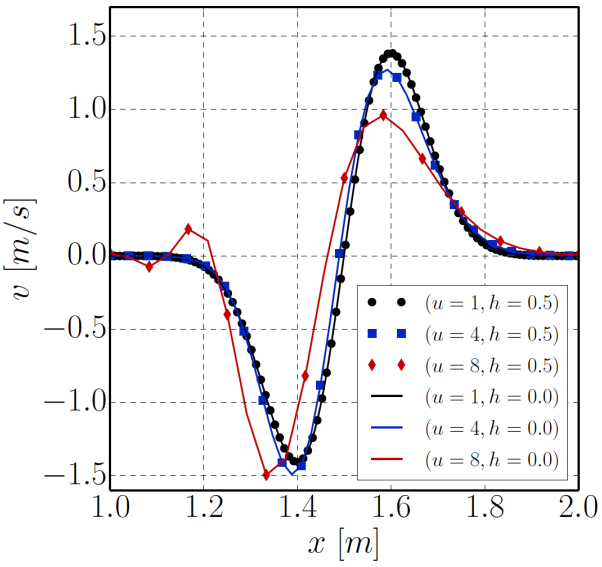

*Figure 6. Comparison with the **elsA** software. Different values of coarsening ratio along the x-axis. Similar results are found, whatever the value of h. However, a high coarsening ratio implies instabilities and dispersion.*

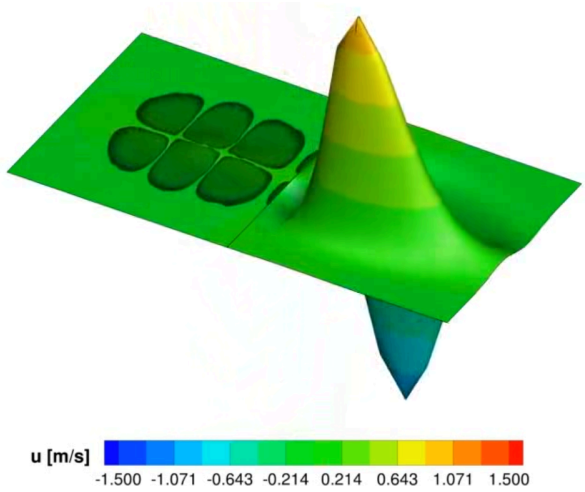

Figure 7. Convection of an isentropic compressible vortex through a nonconforming grid interface with a high coarsening ration (u = 40) between the well refined left block and the coarse right block. High frequency waves are reflected by the interface.

Analogously to electromagnetic waves, a reflected wave is created to satisfy the boundary conditions (related to the numerical scheme) at the interface separating two media of different refractive indices.

4. METRIC CORRECTION

The high-frequency waves reflection is totally unacceptable since it pollutes the upstream flow, which is computed on a well-refined mesh. In this section, a method is described to avoid the reflection. It is a based on a Riemann solver at the interface. Two steps are necessary to implement a Riemann solver. The first one, which is the key point of the solution, is the metric-dependent third-order interpolation to evaluate the left and the right state at the interface. Then, the second one is the Riemann solver based on the Roe's schemes [30]. All the details about this interpolation are given in [1]. The left state interpolation is given by:

$$f^{L}_{i+1/2} = \frac{9u+1}{6(u+1)} f_i + \frac{8}{3(u+1)(u+3)} f_{i+1} - \frac{3u+1}{6(u+3)} f_{i-1}. \quad (15)$$

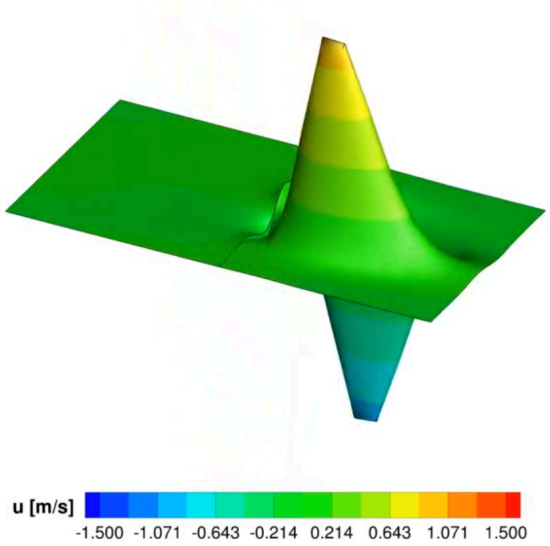

Figure 8. Convection of an isentropic compressible vortex through a nonconforming grid interface with a high coarsening ration (u = 40) between the well refined left block and the coarse right block. The vortex is perfectly convected thanks to the metric correction.

Since the stencil is not symmetric because of the mesh coarsening, the interpolation is not symmetric and the right state interpolation is given by:

$$f^{R}_{i+1/2} = \frac{7u^2-3u+6}{6u(u+1)} f_{i+1} + \frac{4u(3-u)}{3(u+1)(3u+1)} f_i - \frac{5u^2-3u+6}{6u(3u+1)} f_{i+2}. \quad (16)$$

This correction has been implemented inside the ***elsA*** software and the result is given in Fig. 8.

5. CONCLUSION

The aim of the present work was to study the nonconforming grid interface and its stability when used in unsteady simulations (Unsteady Reynolds Average Navier-Stokes, LES with low-order schemes) on multi-domain and multi-scale meshes. The main default of non-matching joins is that they have been developed for steady simulations. As seen previously, they cannot be simply extended to unsteady simulations without any particular precautionary measures. The stability of a numerical scheme plays a key role. Nobody needed reminding of Lax's theorem which ensures the convergence if the numerical scheme is stable and consistent. This study was carried out through spectral analysis. This kind of study allows characterizing the dissipation and the dispersion of the numerical scheme, which is essential for convecting wave packets for example. This analysis was performed theoretically and numerically on a simple configuration (CO-VO).

6. REFERENCES

[1]. Vanharen, J., Puigt, G., Montagnac, M. (2015). Theoretical and numerical analysis of nonconforming grid interface for unsteady flows. *J. Comput. Phys.* **285**, 111-132.

[2]. Mavriplis, D.J. (1997). Unstructured grid techniques. *Annu. Rev. Fluid Mech.* **29**, 473-514.

[3]. Landmann, B., Montagnac, M. (2011). A highly automated parallel chimera method for overset grids based on the implicit hole cutting technique. *Int. J. Numer. Methods Fluids* **66**(6), 778-804.

[4]. Puigt, G., Gazaix, M., Montagnac, M., Le Pape, M.-C., de la Llave Plata, M., Marmignon, C., Boussuge, J.-F., Couaillier, V. (2011). Development of a new hybrid compressible solver inside the CFD ***elsA*** software. In Proc. 20th Computational Fluid Dynamics Conference, American Institute of

Aeronautics and Astronautics, Honolulu (HI), USA, no. AIAA-2011-3379.

[5]. Kao, K.-H., Liou, M.-S. (1995). Advance in overset grid schemes - from Chimera to DRAGON grids. *AIAA J.* **33**(10), 1809-1815.

[6]. Rai, M. M. (1986). A conservative treatment of zonal boundaries for Euler equation calculations. *J. Comput. Phys.* **62**(2), 472-503.

[7]. Rai, M. M. (1986). A relaxation approach to patched-grid calculations with the Euler equations. *J. Comput. Phys.* **66**(1), 99-131.

[8]. Rai, M.M. (1986). An implicit, conservative, zonal-boundary scheme for Euler equation calculations. *Comput. Fluids* **14**(3), 295-319.

[9]. Rai, M.M. (1989). Three-dimensional Navier-Stokes simulations of turbine rotor-stator interaction. Part II – results. *J. Propuls. Power* **5**(3), 312-319.

[10]. Biedron, R., Thomas, J. (1990). A generalized patched-grid algorithm with application to the F-18 forebody with actuated control strake. *Comput. Syst. Eng.* **1**(2–4), 563-576.

[11]. Vichnevetsky, R., Bowles, J.B. (1982). Fourier analysis of numerical approximations of hyperbolic equations. *SIAM Stud. Appl. Math.*

[12]. Vichnevetsky, R. (1981). Propagation through numerical mesh refinement for hyperbolic equations. *Math. Comput. Simul.* **23**(4), 344-353.

[13]. Vichnevetsky, R. (1981). Energy and group velocity in semi discretizations of hyperbolic equations. *Math. Comput. Simul.* **23**(4), 333-343.

[14]. Poinsot, T. J., Lele, S. K. (1992). Boundary conditions for direct simulations of compressible viscous flows. *J. Comput. Phys.* **101**(1), 104-129.

[15]. Lele, S.K. (1992). Compact finite difference schemes with spectral-like resolution. *J. Comput. Phys.* **103**(1), 16-42.

[16]. Kim, J., Lee, D. (1996). Optimized compact finite difference schemes with maximum resolution. *AIAA J.* **34**(5), 887-893.

[17]. Lerat, A., Wu, Z. (1996). Stable conservative multidomain treatments for implicit Euler solvers. *J. Comput. Phys.* **123**(1), 45-64.

[18]. Berland, J., Bogey, C., Marsden, O., Bailly, C. (2007). High-order, low dispersive and low dissipative explicit schemes for m–ultiple-scale and boundary problems. *J. Comput. Phys.* **224**(2), 637-662.

[19]. Epstein, B., Peigin, S. (2010). Treatment of nonmatched grids for high-accuracy Navier-Stokes solutions. *AIAA J.* **48**(7), 1542-1553.

[20]. Rumsey, C. L. (1996). Computation of acoustic waves through sliding-zone interfaces using an Euler/Navier-Stokes code. *AIAA J.* **35**, 263-268.

[21]. Thompson, K. W. (1987). Time dependent boundary conditions for hyperbolic systems. *J. Comput. Phys.* **68**(1), 1-24.

[22]. Fosso Pouangué, A., Deniau, H., Lamarque, N. (2010). A sixth-order compact finite-volume scheme for aeroacoustics: application to a Large Eddy Simulation of a jet. In V European Conference on Computational Fluid Dynamics, ECCOMAS CFD, Lisbon, Portugal.

[23]. Cambier, L., Heib, S., Plot, S. (2013). The Onera elsA CFD software: input from research and feedback from industry. *Mech. Ind.* **14**(3), 159-174.

[24]. Tam, C. K., Webb, J.C. (1993). Dispersion-relation-preserving finite difference schemes for computational acoustics. *J. Comput. Phys.* **107**(2), 262-281.

[25]. Bogey, C., Bailly, C. (2004). A family of low dispersive and low dissipative explicit schemes for flow and noise computations. *J. Comput. Phys.* **194**(1), 194-214.

[26]. Wang, Z. J., Fidkowski, K., Abgrall, R., Bassi, F., Caraeni, D., Cary, A., Deconinck, H., Hartmann, R., Hillewaert, K., Huynh, H. T., Kroll, N., May, G., Persson, P. O., Van Leer, B., Visbal, M. (2013). High-order CFD methods: current status and perspective. *Int. J. Numer. Methods Fluids* **72**(8), 811-845.

[27]. Kim, J. W., Lee, D.J. (2000). Generalized characteristic boundary conditions for computational aeroacoustics. *AIAA J.* **38**(11), 2040- 2049.

[28]. Kim, J. W., Lee, D. J. (2003). Characteristic interface conditions for multiblock high-order computation on singular structured grid. *AIAA J.* **41**(12), 2341-2348.

[29]. Bocquet, S., Sagaut, P., Jouhaud, J. C. (2012). A compressible wall model for Large-Eddy Simulation with application to prediction of aerothermal quantities. *Phys. Fluids* **24**(6).

[30]. Roe, P. L. (1981). Approximate Riemann solvers, parameter vectors, and difference schemes. *J. Comput. Phys.* **43**(2), 357-372.